# Neutron capture cross sections of $^{130,132,134,136,138}$Ba

A. Y. Dauenhauer and K. S. Krane
*Department of Physics, Oregon State University, Corvallis, Oregon 97331, USA*
(Received 17 December 2010; revised manuscript received 1 March 2012; published 4 June 2012)

Cross sections for radiative capture of neutrons have been measured by the activation technique for stable isotopes of Ba with mass numbers 130, 132, 134, 136, and 138. From separate irradiations using thermal and epithermal neutrons, independent values for the thermal cross sections and effective resonance integrals have been determined. Improved values for the radioactive decay half-lives of $^{131}$Ba$^{g}$, $^{131}$Ba$^{m}$, $^{133}$Ba$^{m}$, $^{135}$Ba$^{m}$, and $^{139}$Ba were also obtained. Results of a new measurement of the energies and intensities of the $\gamma$ rays in the decay of $^{139}$Ba are reported, along with $\beta$ feedings and energies for the excited states in the daughter $^{139}$La.

DOI: 10.1103/PhysRevC.85.064301 PACS number(s): 25.40.Lw, 27.60.+j, 23.20.Lv

## I. INTRODUCTION

Neutron capture cross sections offer insight into basic nuclear structure but also have important applications in forensic science (for example, neutron activation analysis), medicine, astrophysics, and geochemistry. The Ba isotopes, in particular, offer many examples of the importance of accurate and systematic knowledge of the cross sections. The approach across the stable Ba isotopes toward semimagic $^{138}$Ba illustrates the influence of shell effects on the cross section. At intermediate energies, neutron capture by the stable Ba isotopes can illuminate the $s$-process path of nucleosynthesis [1]. Neutron capture by $^{130}$Ba with the subsequent decay of $^{131}$Ba is currently the principal means of producing the radioactive daughter $^{131}$Cs, which is widely used for brachytherapy in treating a variety of cancers [2]. The final product of this same decay chain is stable $^{131}$Xe, which is found in unusually high concentrations in lunar rocks and which is most likely produced as a result of resonance neutron capture in $^{130}$Ba [3,4].

Neutron capture by the even-mass isotopes of naturally occurring Ba (mass numbers 130, 132, 134, 136, 138) produces a range of radioisotopes from $^{131}$Ba to $^{139}$Ba, most with low-spin ground states and high-spin metastable states, and encompassing a range of half-lives from 2.5 min to 10 yr. Previous measurements [5,6] of the Ba neutron capture cross sections for thermal and epithermal neutrons have not produced a convergent set of values, and none of the previous measurements offers a broad set of results covering capture by all of the available Ba isotopes. Results of measurements of individual cross sections in this sequence by different investigators are generally in very poor agreement with one another, differing by factors of 2 or more. There are few recent measurements, and older values in the literature are often based on decay parameters such as half-lives and $\gamma$-ray branching intensities that have been superseded by more precise values.

In the present work we have undertaken a systematic study of the neutron capture cross sections for the Ba isotopes, including the production of both radioactive ground and metastable states. Because the resonance integral is typically an order of magnitude larger than the thermal cross section, extraction of the thermal cross section from capture data usually requires precise and reliable values of the resonance integrals. The results of our measurements of the thermal cross sections and resonance integrals of the Ba isotopes are included in the present paper. In the process of observing the radioactive decays to determine the cross sections, we have also determined improved values for the decay half-lives of several of the Ba radioisotopes, which are included in this paper.

In the $\beta$ decay of $^{139}$Ba, the 83rd neutron transforms to a proton, resulting in the semimagic $^{139}$La. The $\beta$ decays populate several excited states in $^{139}$La through first-forbidden transitions. From a careful study of the energies and intensities of the $\gamma$ rays emitted in the $^{139}$Ba decay, we have determined an improved set of values of the energy levels in $^{139}$La and the corresponding log $ft$ values of the $\beta$ decays leading to those states.

## II. EXPERIMENTAL DETAILS

Samples of $Ba(NO_3)_2$ powder of natural isotopic abundance ranging from 10 to 100 mg were irradiated in the Oregon State University TRIGA reactor [7]. Four different irradiation facilities were used: a thermal column (TC; nominal thermal and epithermal neutron fluxes of, respectively, $9.0 \times 10^{10}$ and $2.0 \times 10^{8}$ neutrons cm$^{-2}$ s$^{-1}$), an in-core irradiation tube (ICIT; $4.3 \times 10^{12}$ and $3.9 \times 10^{11}$ neutrons cm$^{-2}$ s$^{-1}$), a cadmium-lined in-core irradiation tube (CLICIT; 0 and $1.2 \times 10^{12}$ neutrons cm$^{-2}$ s$^{-1}$), and a fast pneumatic transfer facility ("rabbit"; $8.3 \times 10^{12}$ and $3.3 \times 10^{11}$ neutrons cm$^{-2}$ s$^{-1}$). Some rabbit samples were enclosed in a Cd box (1 mm wall thickness) to isolate the epithermal component.

Each irradiation was accompanied by several samples of known cross sections that served as monitors of the neutron flux. Primary flux monitors were Au and Co as dilute (respectively, 0.134% and 0.438%) alloys in thin Al metal foils. In our analysis we have assumed the thermal cross section and resonance integral of Au to be, respectively, $98.65 \pm 0.09$ b and $1550 \pm 28$ b and those of Co to be, respectively, $37.18 \pm 0.06$ b and $74 \pm 2$ b [5]. Zr served as a secondary flux monitor, especially for correcting for the small epithermal components in the TC and rabbit facilities. Irradiations for the cross section measurements typically lasted 1–3 h in the ICIT, CLICIT, and TC facilities, and counting began about 4 h after the irradiations. Irradiations in the rabbit facility were of

 ©2012 American Physical Society

duration 1–2 min, and counting began a few minutes after the irradiations.

The $\gamma$ rays were observed with a high-purity Ge detector (nominal volume of 169 $cm^3$, efficiency of 35% compared with NaI at 1332 keV, resolution of 1.68 keV at 1332 keV). Source-to-detector distances for the cross section measurements were generally 10–20 cm, for which coincidence summing effects are negligible. The signals were analyzed with a digital spectroscopy system connected to a desktop computer. Peak areas of the $\gamma$-ray lines, which were well isolated from neighboring peaks, were determined with the ORTEC MAESTRO software [8].

Parameters used in the analysis of the Ba cross sections are shown in Table I. Isotopic abundances are taken from the current recommended values of the IUPAC Commission on Isotopic Abundances and Atomic Weights [9]. Decay half-lives are from the Evaluated Nuclear Structure Data File (ENSDF) [10] for $^{133}Ba^{g}$ and $^{137}Ba^{m}$, with the remainder being new values deduced from the present work. Branching ratios of the $\gamma$ rays are from the ENSDF.

After correcting for the decay of the sample and the $\gamma$-ray branching and efficiency factors, the deduced activities were analyzed according to the result of solving the rate equation for a simple capture and decay process, for which the activity $a$ is

$$a = N(\sigma\phi_{\text{th}} + I\phi_{\text{epi}})(1 - e^{-\lambda t_{\text{i}}}), \tag{1}$$

where $N$ (assumed to be constant) is the number of stable Ba target nuclei in the irradiated sample, $\phi_{\text{th}}$ and $\phi_{\text{epi}}$ are the thermal and epithermal neutron fluxes, $\sigma$ and $I$ are, respectively, the effective thermal cross section and resonance integral, and $t_{\text{i}}$ is the irradiation time.

For irradiations in the thermal column, where the flux is nearly Maxwellian, the effective thermal cross section $\sigma$ is essentially identical to $\sigma_0$, the 2200-m/s cross section (assuming the thermal cross section is proportional to $1/v$). For irradiations in the reactor core, the effective $\sigma$ is larger than $\sigma_0$ by about 1.5%.

Because there are no broad or low-lying neutron resonances known for any of the Ba isotopes considered in the present work (with the possible exception of $^{138}$Ba), the cross section closely follows the $1/v$ behavior below about 1 eV. Therefore the effective thermal cross section characterizes the entire thermal region. (This is equivalent to setting Wescott's $g$ factor equal to unity [11].) The effects of neutron absorption within the samples are also negligible, given the thin samples used in the present experiments.

The effective resonance integral $I$ includes a small contribution from the $1/v$ region. Assuming the Cd cut-off energy to be about 0.5 eV, this contribution amounts to about $0.45\sigma$ and the corrected resonance integral $I'$ is then

$$I' = I - 0.45\sigma. \tag{2}$$

Because the resonance integral is generally much larger than the thermal cross section, this amounts to a small correction that is at most one standard deviation of $I$, except for $^{138}$Ba, an unusual case in which the resonance integral is slightly smaller than the thermal cross section, in which case Eq. (2) produces a very large correction to the measured value of $I$ (roughly 50%).

Uncertainties in the cross sections depend on a number of factors: isotopic abundance, half-life, flux determinations (including corrections of thermal cross sections for the presence of epithermal neutrons), detector efficiencies, and decay scheme factors, including $\gamma$-ray branching. Overall these factors combine to give a typical uncertainty of 4–5%. In cases in which one of these factors is especially large (for example, the uncertainty in the branching ratio) or in which the thermal cross section calculated from Eq. (1) has an especially large sensitivity to the resonance integral, the uncertainty may exceed this value.

In cases in which the radioactive ground state is fed through the metastable state ($^{131}$Ba and $^{133}$Ba), the population of the metastable state was determined from its decays, and from that value the number of decays to the ground state during and subsequent to the irradiation was calculated and subtracted from the observed total ground-state population. The resulting value of the ground-state population is thus due only to direct production by neutron capture (that is, without going through the metastable state), which then permits the cross sections for ground-state formation to be deduced.

For the $^{139}$Ba spectroscopy studies, samples of typical initial activity of 750 $\mu$Ci were counted, first at a source-to-detector distance of 25 cm and then moving successively to 20, 15, 10, and 5 cm at intervals of approximately one half-life. This procedure enables sum peaks and long-lived impurities to be readily identified. To reduce the dead time caused by the

TABLE I. Properties of Ba isotopes.

| Capture by | Capture to | Abundance[a] (%) | Half-life[b] | Analyzing $\gamma$ rays[c] |
|---|---|---|---|---|
| $^{130}$Ba | $^{131}Ba^{g}$ | 0.106(1) | 11.52(1) d | 123.8 (29.8%), 216.0 (20.4%), 373.2 (14.4%), 496.3 (48.0%) |
| | $^{131}Ba^{m}$ | | 14.26(9) min | 108.1 (55.4%) |
| $^{132}$Ba | $^{133}Ba^{g}$ | 0.101(1) | 10.51(5) yr[c] | 356.0 (62.1%) |
| | $^{133}Ba^{m}$ | | 38.88(8) h | 275.9 (17.8%) |
| $^{134}$Ba | $^{135}Ba^{m}$ | 2.417(18) | 28.11(2) h | 268.2 (16.0%) |
| $^{136}$Ba | $^{137}Ba^{m}$ | 7.854(24) | 2.552(1) min[c] | 661.7 (89.9%) |
| $^{138}$Ba | $^{139}$Ba | 71.70(4) | 83.25(8) min | 165.9 (23.7%) |

[a]From Berglund and Wieser [9].
[b]Values from present work unless otherwise indicated.
[c]From ENSDF [10].

intense 165.9-keV line, a Pb absorber of 3 mm thickness was placed in front of the detector.

The $\gamma$-ray spectra were analyzed for peak locations and areas using the fitting code SAMPO [12]. Energy calibrations for the spectroscopy studies were done by counting the Ba samples simultaneously with samples of $^{56}$Mn, $^{56,60}$Co, $^{152}$Eu, and $^{207}$Bi [13]. Efficiency calibrations were done with standardized sources of $^{133}$Ba and $^{152}$Eu. The efficiency calibration below 200 keV was also characterized using reactor-produced sources of $^{160}$Tb, $^{169}$Yb, and $^{182}$Ta. The minimum uncertainty in intensities for the spectroscopic studies has been set at 1%. This represents primarily the fitting uncertainty in our efficiency calibrations and below 1500 keV is a more generous estimate that the value of 0.5% suggested by Debertin and Helmer [14] for this energy range under optimum conditions.

## III. HALF-LIVES AND CROSS SECTION RESULTS

A sample $\gamma$-ray spectrum just after an irradiation in the rabbit facility is shown in Fig. 1, illustrating the prominent peaks in the short-lived Ba activities. Figure 2 shows a spectrum several hours after a core irradiation, illustrating peaks from the longer-lived Ba isotopes.

### A. Half-lives

Before analyzing the cross sections, it is necessary to have precise values for the radioactive decay half-lives. We have remeasured the half-lives of five of the seven activities used in the present studies (all except $^{133}$Ba$^g$ and $^{137}$Ba$^m$). A $^{60}$Co source served as a dead-time monitor for the half-life measurements. The deduced values from the present work were presented in Table I.

*$^{131}Ba^g$*. Our $^{131}$Ba$^g$ half-life of 11.52 ± 0.01 d was deduced by following the 123.8, 216.0, 373.2, and 496.3 keV $\gamma$ rays for at least two half-lives from several different samples. This value agrees with and is more precise than the most recent value in the literature, 11.50 ± 0.06 d, reported by Bode *et al.* [15]. The value of Bode *et al.* was smaller than the previously reported values, but we agree with their value.

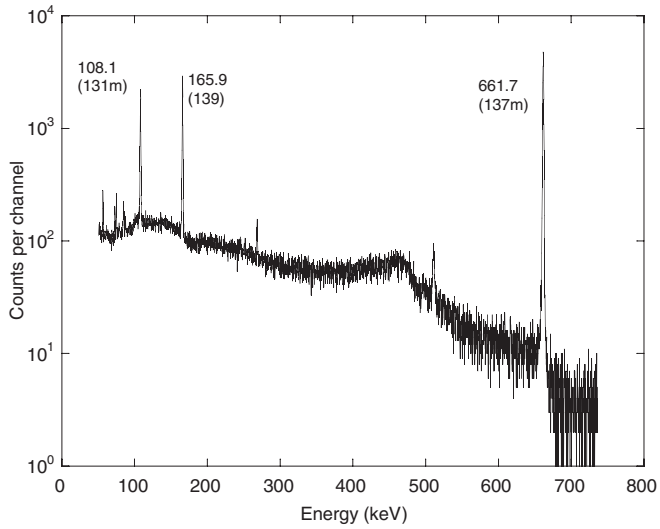


FIG. 1. $\gamma$-ray spectrum from short-lived isotopes in irradiated Ba just after rabbit irradiation. Labeled lines were used for cross section evaluation.

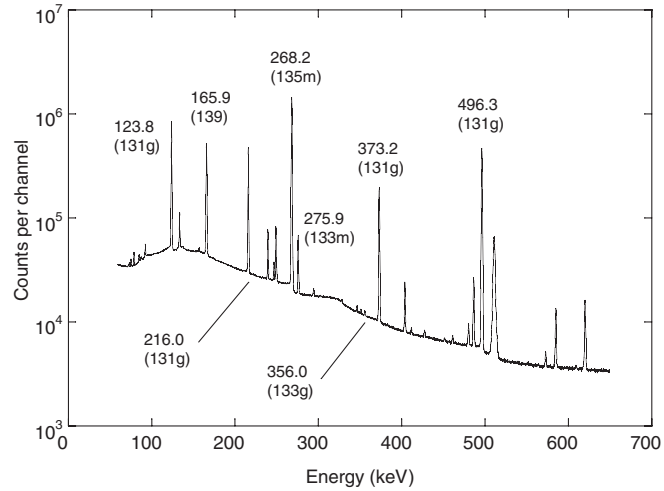


FIG. 2. $\gamma$-ray spectrum of irradiated Ba following core irradiation showing lines from longer-lived isotopes used for cross-section evaluation.

*$^{131}Ba^m$*. There is only one previous report of a measurement of the half-life of $^{131}$Ba$^m$, 14.6 ± 0.2 min by Horen *et al.* [16]. They produced their activity through a charged-particle reaction, so the present report is the first half-life measurement in which the activity was obtained from neutron capture. The agreement between the older value and our new and more precise value, 14.26 ± 0.09 min, is good.

*$^{133}Ba^m$*, *$^{135}Ba^m$*. The presently accepted values of the $^{133}$Ba$^m$ and $^{135}$Ba$^m$ half-lives were reported by Willie and Fink [17]. Our value for the $^{133}$Ba$^m$ half-life, 38.88 ± 0.08 h, agrees with and is slightly more precise than their value 38.9 ± 0.1 h, while our value for $^{135}$Ba$^m$, 28.11 ± 0.02 h is an order of magnitude more precise but somewhat smaller than their value, 28.7 ± 0.2 h.

*$^{139}Ba$*. Our value for the $^{139}$Ba half-life, 83.25 ± 0.08 min, was arrived at by following several samples over four half-lives. It agrees with and is more precise than the previously adopted value, 83.06 ± 0.28 min, which was reported by Gehrke [18]. However, as discussed by the ENSDF, the various measurements fall into two mutually consistent groups that disagree with one another.

### B. Cross sections

Based on the newly measured values for the half-lives, along with the other data listed in Table I, we can now discuss the results of the cross section measurements. Values for the thermal cross sections and resonance integrals (including the $1/v$ contribution, unless otherwise noted) are summarized in Table II, along with the ratio $I/\sigma$ from the present work.

*$^{130}Ba \rightarrow {}^{131}Ba^m, {}^{131}Ba^g$*. For the analysis of the formation of $^{131}$Ba$^m$, it was necessary to apply a small correction, amounting to no more than 10%, to account for the self-absorption of the 108.1-keV $\gamma$ ray in our samples. Our results for the cross

TABLE II. Cross sections of Ba isotopes.

| Process | Thermal cross section $\sigma$ (b) | | Resonance integral $I$ (b) | | $I/\sigma$ |
|---|---|---|---|---|---|
| | Present work | Previous work | Present work | Previous work | |
| $^{130}$Ba → $^{131}$Ba$^m$ | 0.596(37) | 2.5(3),[a] 0.98(5)[b] | 19.3(9) | 23(1)[b] | 32.4(25) |
| $^{130}$Ba → $^{131}$Ba$^g$ | 7.15(34) | 6.42(40),[b] 8.8(9)[c] | 178(10) | 153(7),[b] 270(70)[j] | 24.9(18) |
| $^{132}$Ba → $^{133}$Ba$^m$ | 0.682(29) | 4.1(15),[d] <0.15[e] | 4.32(22) | | 6.33(42) |
| $^{132}$Ba → $^{133}$Ba$^g$ | 7.51(32) | ≈6[f] | 42.5(22) | 24(16)[k] | 5.66(38) |
| $^{134}$Ba → $^{135}$Ba$^m$ | 0.0334(24) | − 0.06(3),[b] <0.05,[d] 0.158(24)[e] | 13.3(8) | 10.6(3)[b] | 398(37) |
| $^{136}$Ba → $^{137}$Ba$^m$ | 0.0287(57) | 0.016(5),[d] 0.011(1),[g] 0.0095(10)[h] | 3.49(17) | | 122(25) |
| $^{138}$Ba → $^{139}$Ba | 0.404(18) | 0.447(7), [b] 0.23(2),[c] 0.36(4),[g] 0.53(1)[i] | 0.382(20) | 0.256(50),[b] 0.380(5),[i] 0.20(9)[l] | 0.946(65) |

[a]Tilbury and Kramer [19].
[b]Heft [20].
[c]Lyon [21].
[d]Hans *et al*. [26].
[e]Mangal and Gill [27].
[f]Katcoff [28].
[g]Kramer and Wahl [30].
[h]Foglio Para and Mandelli Bettoni [31].
[i]Agbemava *et al*. [32].
[j]Steinnes [22].
[k]Masyanov and Anufriev [29].
[l]Ricabarra *et al*. [33] (reduced value $I'$).

sections leading to production of the isomer are

$$\sigma = 0.596 \pm 0.037 \text{ b}, \quad I = 19.3 \pm 0.9 \text{ b}.$$

These cross sections have been previously reported by Tilbury and Kramer [19] using Ba enriched in $^{130}$Ba and by Heft [20] using natural Ba. Tilbury and Kramer determined their thermal cross section, 2.5 ± 0.3 b, from a measurement of the Cd ratio (ratio of activity produced by unshielded and Cd-shielded samples), while Heft determined both the thermal cross section, 0.98 ± 0.05 b, and the resonance integral, 23 ± 1 b, from individual measurements with thermal and epithermal neutrons, analogous to the present method. The discrepancy between Heft's values and ours can be ascribed to the difference between the branching ratios used in the analyses: Heft used a value of 40% while the present work uses the currently accepted value of 55%. If we had used a branching ratio of 40% in our analysis, we would have deduced a resonance integral of 25 b and a thermal cross section of 1.0 b, which would agree with Heft's values obtained with the 40% branching ratio.

These values of the cross sections for the formation of the isomer can then be used to subtract out the contribution to the ground-state activation resulting from decays of the isomer, which results in the following values for the cross section for direct production of the ground state, based on thermal neutron data from the TC, ICIT, and rabbit facilities and on epithermal neutron data from the CLICIT and rabbit facilities:

$$\sigma = 7.15 \pm 0.34 \text{ b}, \quad I = 178 \pm 10 \text{ b}.$$

Heft reports smaller values for these cross sections (respectively, 6.52 ± 0.40 b and 153 ± 7 b). The small differences between Heft's values and the present ones can possibly be traced to Heft's use of larger values for the isomeric cross section to correct for production of the ground state. Other values [21,22] quoted in Table II are consistent with the present ones.

Measurements of the ratio $I/\sigma$ for the ground state have been reported by Van der Linden *et al*. [23] (25.1 ± 0.8) and by St-Pierre and Kennedy [24] (21.6 ± 0.5). These are in good agreement with the ratio of the values determined in the present work. However, the ratio between the isomeric and total (ground + isomeric) cross sections determined from the present results, 0.077 ± 0.006, disagrees with the value measured by Gangrsky *et al*. [25], 0.20 ± 0.02.

$^{132}Ba \rightarrow {}^{133}Ba^m, {}^{133}Ba^g$. We have determined the thermal cross section of the isomeric state from three independent measurements (TC, ICIT, and rabbit) and the resonance integral from two measurements (CLICIT and rabbit). The average of these measurements gives

$$\sigma = 0.682 \pm 0.029 \text{ b}, \quad I = 4.32 \pm 0.22 \text{ b}.$$

The extreme discrepancy between the previously reported values of this thermal cross section (4.1 ± 1.5 b by Hans *et al.* [26] and <0.15 b by Mangal and Gill [27]) with one another as well as with the present results is probably due to the difficulty of accounting for the overlapping contributions to the $\gamma$-ray spectrum of irradiated natural Ba in the NaI detectors used in the previous work.

The cross sections leading to the ground state, after correcting for ground-state production through the isomer, are

$$\sigma = 7.51 \pm 0.32 \text{ b}, \quad I = 42.5 \pm 2.2 \text{ b}.$$

No previous measurements of these cross sections have been reported, although Katcoff [28] observed a long-lived (>20 yr) component of irradiated Ba and assigned it to the decay of $^{133}$Ba$^{g}$, thereby deducing a minimum cross section of about 6 b. Based on a determination of the $^{132}$Ba resonance parameters, Masyanov and Anufriev [29] calculated a value for the resonance integral of 24 ± 16 b, which is consistent with the present result.

For the isomeric state, the ratio $I/\sigma$ has been reported as 5.6 ± 0.3 by Van der Linden *et al.*, which agrees well with the value from the present results. The ratio between the isomeric and total (isomeric + ground) thermal cross sections was determined to be 0.085 ± 0.008 by Gangrsky *et al.* [25], which agrees very well with the value 0.083 ± 0.005 from the present results.

$^{134}Ba \rightarrow {}^{135}Ba^{m}$. The primary determination of this thermal cross section comes from our TC data, because the large resonance integral causes a significant correction in the ICIT and rabbit data. (Even in the TC, the epithermals contribute about 50% to the activation and about 6% to the uncertainty of the deduced thermal cross section.) The resulting cross sections are

$$\sigma = 0.0334 \pm 0.0024 \text{ b}, \quad I = 13.3 \pm 0.8 \text{ b}.$$

Heft [20] obtained a comparable value (10.6 ± 0.3 b) for the resonance integral, but in subtracting out the epithermal contributions deduced a negative value (−0.06 ± 0.03 b) for the thermal cross section. The value of the thermal cross section reported by Hans *et al.* [26] (<0.05 b) is consistent with the present value, but the value reported by Mangal and Gill [27] (0.158 ± 0.024 b) is not; however, both of these previous measurements suffered from uncertainties associated with subtracting various contributions to the $\gamma$-ray spectrum observed with NaI detectors.

The ratio $I/\sigma$ was determined by Van der Linden *et al.* [23] to be 151 ± 7, which disagrees with the present value.

$^{136}Ba \rightarrow {}^{137}Ba^{m}$. Owing to the short half-life of $^{137}$Ba$^{m}$ (2.552 min), measurements on this activity were possible only in the rabbit facility, resulting in the following values:

$$\sigma = 0.0287 \pm 0.0057 \text{ b}, \quad I = 3.49 \pm 0.17 \text{ b}.$$

As in the case of $^{135}$Ba$^{m}$, the deduced thermal cross section depends critically on the subtraction of the epithermal component, but unlike that measurement we have no TC data (with its small epithermal component) to pin down a more precise value of $\sigma$. As a result, the uncertainty on our thermal cross section is relatively large (20%). Previously measured values of the thermal cross section include those of Hans *et al.* [26] (0.016 ± 0.005), Kramer and Wahl [30] (0.011 ± 0.001 b, using enriched Ba), and Foglio Para and Mandelli Bettoni [31] (0.0095 ± 0.0010 b, using natural Ba). There are no previous direct measurements of the resonance integral, but Van der Linden *et al.* [23] report $I/\sigma = 68 \pm 4$, in mild disagreement with the present value.

$^{138}Ba \rightarrow {}^{139}Ba$. The thermal cross section for production of $^{139}$Ba was determined from experiments on the TC, ICIT, and rabbit facilities, and the resonance integral from experiments on the CLICIT and rabbit facilities. The average values from these measurements are

$$\sigma = 0.404 \pm 0.018 \text{ b}, \quad I = 0.382 \pm 0.020 \text{ b}.$$

Previous measurements of the thermal cross section encompass a fairly wide range: 0.23 ± 0.02 by Lyon [21], 0.36 ±0.04 by Kramer and Wahl [30], 0.447 ± 0.007 by Heft [20], and 0.53 ± 0.01 by Agbemava *et al.* [32]. The reduced resonance integral (corrected for the $1/v$ tail) was reported by Ricabarra *et al.* [33] as 0.20 ± 0.09 b, in excellent agreement with the value calculated from our data (0.204 ± 0.021 b). The ratio $I/\sigma$ that was measured to be 0.88 ± 0.04 by Van der Linden *et al.* [23] is likewise in excellent agreement with the value deduced from the present data.

## IV. $\gamma$-RAY SPECTROSCOPY

Figure 3 shows a sample of the high-energy region of the $\gamma$-ray spectrum of an irradiated Ba sample, with the 3-mm Pb absorber in place. In all, three separate irradiated Ba samples were counted to analyze the spectroscopy in the decay of $^{139}$Ba. Each sample was counted at several locations from 25 cm to 5 cm from the detector, with the samples being moved closer to the detector after each half-life in order to keep the counting rate roughly uniform. In all, 11 separate counting intervals were processed, each lasting for at least one half-life.

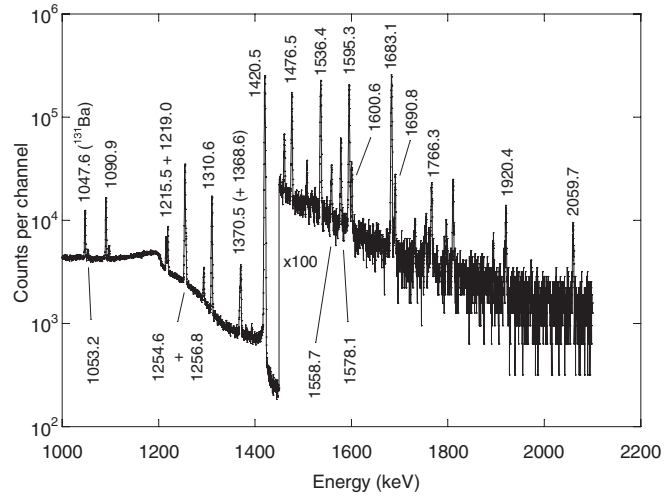


FIG. 3. $\gamma$-ray spectrum of irradiated Ba sample with 3-mm Pb absorber. Lines from the $^{139}$Ba decay are labeled. Other visible lines are from $^{24}$Na (1368.6 keV), $^{56}$Mn (1810.7 keV), and $^{116}$In (1097.3, 1293.6, and 1507.7 keV).

Energies and intensities determined from the 11 data runs were then averaged to obtain the final values reported in this work. Three of the 11 data runs (one for each sample) included the energy calibration sources. These runs were used to establish the energies of the stronger Ba peaks, which were then used as secondary calibration lines to determine the energies of the weaker Ba lines in the runs in which no energy calibration source was present. In this way the weak lines could be analyzed without interference from the calibration sources.

The energy uncertainties in the present work depend on the uncertainties of the calibration lines and the statistical and fitting uncertainties of the Ba lines. The uncertainties of the stronger calibration lines are typically in the range of 1–5 eV [13]. The statistical and fitting uncertainties in our analysis are smaller than 10 eV for the calibration lines in the three calibration data sets and smaller than 20 eV for the stronger Ba lines in all 11 data sets. As a result, the net statistical and fitting uncertainty in the weighted average for the stronger Ba lines would be smaller than 10 eV, and even combining this uncertainty with the energy uncertainty in the calibration lines (regarded as a systematic uncertainty and thus not reducible by averaging multiple data sets) results in a net energy uncertainty below 10 eV for those Ba peaks. However, we feel this is too optimistic a figure for the overall uncertainty and thus in those cases in which the average uncertainty falls below 10 eV we have set the minimum energy uncertainty to be 10 eV.

The $\gamma$-ray energies and intensities (corrected for absorption in the Pb) deduced from the present studies are listed in Table III along with the values from the most recent Nuclear Data Sheets (NDS) compilation [34] (derived from a consensus of the previous measurements by Hill and Wiedenbeck [35], Berzins *et al.* [36], and Laird [37]). Overall our data agree with and are significantly more precise than the NDS results, typically by an order of magnitude or more in both energy and intensity. However, our data disagree in many respects with a more recent measurement of the $\gamma$-ray energies and intensities reported by Zamboni *et al.* [38]. The energies obtained in the present work are in most cases significantly more precise than those of Zamboni *et al.*, whose uncertainties are in the range of 100 eV even for some of the stronger lines of the spectrum. The intensity uncertainties reported by Zamboni *et al.*, on the other hand, are often much smaller than those of the present work, ranging from 0.02% for the stronger lines to 0.3% for some of the weakest lines (of relative intensities

TABLE III. Energies and intensities of $\gamma$ rays emitted in the decay of $^{139}$Ba.

| Previous work[a] | | Present work | | Energy levels (keV) | |
|---|---|---|---|---|---|
| $E$ (keV) | $I$ | $E$ (keV) | $I$ | Initial | Final |
| 165.8575(11) | 9090(92) | 165.825(20) | 9370(100) | 165.858 | 0 |
| 1045.9 | 0.01 | | <0.02 | | |
| 1053.0(5) | 0.12(5) | 1053.162(32) | 0.273(13) | 1219.047 | 165.858 |
| 1090.8(2) | 3.1(3) | 1090.938(10) | 3.80(4) | 1256.797 | 165.858 |
| 1215.5(4) | 1.2(1) | 1215.542(12) | 1.19(2) | 1381.406 | 165.858 |
| 1219.1(4) | 1.5(2) | 1219.044(10) | 1.91(2) | 1219.047 | 0 |
| 1254.7(2) | 10(1) | 1254.631(10) | 11.5(1) | 1420.491 | 165.858 |
| 1256.7(10) | 1.03(12) | 1256.772(22) | 1.44(4) | 1256.797 | 0 |
| 1310.6(2) | 6.1(3) | 1310.617(10) | 5.87(6) | 1476.489 | 165.858 |
| 1370.5(3) | 1.13(11) | 1370.509(10) | 1.04(1) | 1536.387 | 165.858 |
| 1381.5(5) | 0.030(15) | 1381.560(93) | 0.058(4) | 1381.406 | 0 |
| 1392.4(5) | 0.030(15) | 1392.944(75) | 0.050(4) | 1558.721 | 165.858 |
| 1420.5(2) | 100(10) | 1420.478(10) | 100(1) | 1420.491 | 0 |
| 1476.3(3) | 0.61(1) | 1476.488(10) | 0.643(8) | 1476.489 | 0 |
| 1518(1) | <0.02 | 1517.73(18) | 0.018(2) | 1683.144 | 165.858 |
| 1536.3(3) | 0.81(6) | 1536.391(10) | 0.955(10) | 1536.387 | 0 |
| 1558.2(4) | 0.078(30) | 1558.697(31) | 0.108(4) | 1558.721 | 0 |
| 1578.2(4) | 0.20(5) | 1578.146(14) | 0.249(4) | 1578.156 | 0 |
| 1595.3(3) | 0.79(6) | 1595.299(10) | 0.876(9) | 1761.167 | 165.858 |
| 1601.4(10) | 0.05(1) | 1600.577(26) | 0.124(3) | 1766.429 | 165.858 |
| 1683.1(3) | 0.98(5) | 1683.133(10) | 1.16(1) | 1683.144 | 0 |
| 1691.2(10) | 0.11(1) | 1690.750(36) | 0.102(4) | 1856.619 | 165.858 |
| 1754.5(5) | 0.02(1) | 1754.604(82) | 0.040(3) | 1920.432 | 165.858 |
| 1762(1) | 0.03(1) | 1761.18(13) | 0.016(2) | 1761.167 | 0 |
| 1765.5(4) | 0.066(25) | 1766.346(59) | 0.099(5) | 1766.429 | 0 |
| 1797.4(10) | 0.02(1) | 1796.97(11) | 0.024(2) | 1962.84 | 165.858 |
| 1894.7(7) | 0.008(6) | 1894.28(13) | 0.015(2) | 2059.899 | 165.858 |
| 1920.6(4) | 0.030(14) | 1920.407(42) | 0.062(3) | 1920.432 | 0 |
| 2060.1(4) | 0.019(9) | 2059.72(10) | 0.043(3) | 2059.899 | 0 |

[a]From NDS compilation [34].

TABLE IV. Energy levels of $^{139}$La populated in the decay of $^{139}$Ba.

| Previous work[a] | | | | Present work | | |
|---|---|---|---|---|---|---|
| $E$ (keV) | $J^\pi$ | $I_\beta$ | log $ft$ | $E$ (keV) | $I_\beta$ | log $ft$[c] |
| 0.000 | $7/2^+$ | 69.98(31) | 6.847(4) | 0.000 | 69.98(31)[a] | 6.848(3) |
| 165.8576(11) | $5/2^+$ | 29.68(31) | 7.089(6) | 165.8576(11)[b] | 29.69(31) | 7.090(5) |
| 1219.0(4) | $9/2^+$ | 0.0042(7) | 9.81(8) | 1219.047(10) | 0.00554(9) | 9.690(9) |
| 1256.66(20) | $(5/2)^+$ | 0.0108(14) | 9.34(6) | 1256.797(10) | 0.0133(2) | 9.253(8) |
| 1381.4(4) | $(9/2)^+$ | 0.0032(5) | 9.67(7) | 1381.406(12) | 0.00317(7) | 9.677(11) |
| 1420.54(15) | $5/2^+$,$7/2^+$ | 0.287(7) | 7.652(12) | 1420.491(10) | 0.283(4) | 7.659(8) |
| 1476.42(17) | $(9/2^+)$ | 0.0175(20) | 8.77(5) | 1476.489(10) | 0.0165(3) | 8.793(10) |
| 1536.34(22) | $7/2^+$ | 0.0051(6) | 9.19(6) | 1536.387(10) | 0.00506(7) | 9.192(9) |
| 1558.2(4) | $3/2^+$,$5/2^+$ | 0.00028(10) | 10.40(16) | 1558.721(29) | 0.000401(15) | 10.248(18) |
| 1578.2(4) | $5/2^+$,$7/2^+$ | 0.00052(14) | 10.09(12) | 1578.156(14) | 0.000632(13) | 10.010(11) |
| 1683.1(3) | $7/2^+$ | 0.0026(3) | 9.16(5) | 1683.144(10) | 0.00299(4) | 9.102(10) |
| 1761.2(3) | | 0.0021(3) | 9.06(7) | 1761.167(10) | 0.00226(5) | 9.028(13) |
| 1765.8(4) | $3/2^+$,$5/2^+$ | 0.00030(8) | 9.89(12) | 1766.429(24) | 0.000566(16) | 9.615(15) |
| 1857.1(10) | $3/2^+$,$5/2^+$ | 0.00029(4) | 9.64(6) | 1856.619(36) | 0.000259(11) | 9.691(21) |
| 1920.5(4) | $(7/2^+)$ | 0.00013(5) | 9.77(17) | 1920.432(37) | 0.000259(11) | 9.475(22) |
| 1963.3(10) | $(5/2)^+$ | 0.00005(3) | 10.0(3) | 1962.84(11) | 0.000061(5) | 9.94(4) |
| 2060.2(4) | | 0.0007(3) | 9.43(19) | 2059.899(79) | 0.000147(9) | 9.11(4) |

[a]From NDS compilation [34].
[b]From Alburger and Wesselborg [40].
[c]Assuming nonunique decays.

<0.1%). Such small intensity uncertainties are inconsistent with limits recommended by Debertin and Helmer [14] based on efficiency calibrations (0.5%–1%) and also far smaller than those found in collections of $\gamma$-ray intensity calibration standards (see, for example, Meyer [39]), which typically show intensity uncertainties ranging from 0.5% to 1% for the strongest lines to 5%–10% for the weaker lines with branching ratios of 0.01%–0.1%.

More than 99% of the $^{139}$Ba $\beta$-decay intensity directly populates the ground and first-excited states in $^{139}$La. The remaining 0.33% of the decay intensity is divided among first-forbidden transitions to many states in the 1–2 MeV region. Most of these states show $\gamma$ decays to both the ground and first-excited states, as listed in Table III. From the $\gamma$-ray energies we have determined a set of values of the excited-state energies (taking the energy of the first-excited state as 165.8575 $\pm$ 0.0011 keV from the precise measurement by Alburger and Wesselborg [40]), and from the $\gamma$ intensities we have deduced the $\beta$ decay feedings to the excited states, which are shown in Table IV. (In our analysis we have assumed the NDS value for the ground-state $\beta$ intensity.) We have obtained an improvement by an order of magnitude or more in the precision of the excited-state energies and the $\beta$ intensities, compared with the previous NDS compilation.

Conspicuously absent from the pattern of decays of the 1–2 MeV excited states to both the ground and first-excited states are transitions of energy 1412.298 keV (from 1578.156 keV to the first-excited state) and 1865.619 and 1962.84 keV (from the corresponding excited states to the ground state). Our spectra show no evidence for those transitions (even though they are not forbidden by the proposed spin assignments), and we obtain upper limits on their intensities, respectively, of 0.015, 0.005, and 0.004.

## V. DISCUSSION

We have achieved a systematic study by activation of the cross sections of all radioactive ground states and metastable states produced following neutron capture by natural Ba (except the 0.3-s metastable state in $^{136}$Ba, which is not observable in our measurements). By measuring in different reactor environments with varying thermal and epithermal fluxes, we have been able to correct for captures by epithermal neutrons and so deduce a set of unambiguous thermal cross sections, all obtained using the most precise and current values of the isotopic abundances, half-lives, and branching ratios. In addition, we have remeasured several half-lives to greater precision than previous values and performed a detailed remeasurement of the energies and intensities of the $\gamma$ rays in the decay of $^{139}$Ba using multiple sources for energy and intensity calibrations.

It is interesting to compare the cross sections determined by activation with those deduced from observation of the primary $\gamma$ rays following neutron capture leading to the same final states in the Ba isotopes. Such a comparison is shown in Table V, based on the cross sections from primary $\gamma$ rays reported for $^{135}$Ba$^m$ by Bondarenko *et al.* [41] and tabulated for other Ba isotopes by Firestone *et al.* [42] The agreement between the two methods is satisfactory for $^{135,137,139}$Ba, but poor for $^{131}$Ba. The explanation for the discrepancy is not apparent. The activation measurement depends critically on the knowledge of the absolute intensity of the 108-keV $\gamma$ ray from

TABLE V. Comparison of thermal cross sections from activation and from primary $\gamma$ rays.

| Final nuclide | Thermal cross section $\sigma$ (b) deduced from | |
|---|---|---|
| | Activation | Primary $\gamma$ rays |
| $^{131}$Ba$^{m}$ | 0.596(37) | 4.4(4)[a] |
| $^{131}$Ba$^{g}$ | 7.15(34) | |
| $^{133}$Ba$^{m}$ | 0.682(29) | |
| $^{133}$Ba$^{g}$ | 7.51(32) | |
| $^{135}$Ba$^{m}$ | 0.0334(24) | 0.046(3)[a], 0.11(2)[b] |
| $^{137}$Ba$^{m}$ | 0.0287(57) | 0.020(4)[a] |
| $^{139}$Ba | 0.404(18) | 0.435(12)[a] |

[a]From Firestone *et al*. [42].
[b]From Bondarenko *et al*. [41].

the decay of the $^{131}$Ba$^{m}$ metastable state, which was deduced in a 1963 measurement by Horen *et al*. [16]. However, that intensity would need to be reduced by an order of magnitude in order to reconcile the two discordant results, which seems unlikely.

The present spectroscopic study of the $^{139}$Ba decay has produced $\gamma$-ray energies and intensities with about an order of magnitude greater precision than the previously accepted data set. Because $^{139}$La has a closed $N = 82$ neutron shell, the ground $(7/2^+)$ and first-excited $(5/2^+)$ states strongly populated in the decay are readily identified with the $g_{7/2}$ and $d_{5/2}$ single-proton states expected for $Z = 57$. Above the first-excited state is a gap of more than 1 MeV, and then there are more than 20 excited states between 1.2 and 2.0 MeV. These states have been variously identified as three quasiparticle configurations [43], as quasiparticle-plus-phonon states [44], and as couplings of a single particle to $sd$ bosons [45]. Several states of each possible spin-parity assignment result from these models, and it may be difficult to sort out the correspondence between the calculated and observed states.

A critical test for these models is the relative photon branching from states of the excited multiplets to the two single-particle states. Table VI shows the crossover-to-cascade intensity ratios $I(J^\pi \to 7/2_1^+)/I(J^\pi \to 5/2_1^+)$ from our radioactive decay data compared with similar values from Coulomb excitation [46] and inelastic neutron scattering [47]. The neutron-scattering work did not report intensities for the cascade transitions from the 1578.2- and 1683.1-keV levels, nor for the crossover transition from the 1962.8-keV level. We have estimated upper limits on those transitions from the inelastic neutron-scattering $\gamma$-ray spectrum [47] to obtain the limits shown in Table VI. The neutron-scattering work also did not report the intensity of the 1254.6-keV cascade transition from the 1420.5-keV level, because it could not be resolved from the 1256.8-keV crossover transition. In the present work, the 1256.8-keV transition appears as an incompletely resolved shoulder on the 1254.6-keV peak; the neutron-scattering work was done at resolution inferior to the present work (3.8 keV), and so the 1254.6- and 1256.8-keV peaks are completely unresolved in that work. In another neutron-scattering study [48], Daniels and Felsteiner observed that half the $\gamma$-ray

TABLE VI. Crossover-to-cascade ratios in $^{139}$La.

| Energy level (keV) | $J^\pi$ | Crossover-to-cascade ratio | | |
|---|---|---|---|---|
| | | $\beta$ decay | CoulEx | $n,n'$ |
| 1219.0 | $9/2^+$ | 7.00(34) | 9.00(91) | 10(4) |
| 1256.8 | $(5/2)^+$ | 0.379(11) | 0.724(21) | 0.38(9) |
| 1381.4 | $(9/2)^+$ | 0.049(3) | | 0.048(7) |
| 1420.5 | $5/2^+,7/2^+$ | 8.70(12) | | 8.0(19) |
| 1476.5 | $(9/2^+)$ | 0.110(2) | | 0.138(21) |
| 1536.4 | $7/2^+$ | 0.918(13) | 1.00(6) | 8.7(12) |
| 1558.7 | $3/2^+,5/2^+$ | 2.16(19) | | 1.36(19) |
| 1578.2 | $5/2^+,7/2^+$ | >17 | | >12 |
| 1683.1 | $7/2^+$ | 64.4(72) | | >12 |
| 1761.2 | | 0.018(2) | | |
| 1766.4 | $3/2^+,5/2^+$ | 0.798(45) | | 1.0(2) |
| 1856.6 | $3/2^+,5/2^+$ | <0.05 | | |
| 1920.4 | $(7/2^+)$ | 1.55(14) | | 1.2(2) |
| 1962.8 | $(5/2)^+$ | <0.17 | | <0.5 |
| 2059.9 | | 2.87(43) | | 1.40(25) |

intensity in the unresolved peak was in coincidence with the 165.9-keV transition. Making a similar assumption that half the intensity observed in Ref. [47] can be assigned to 1254.6 keV and half to 1256.8 keV, we obtain the crossover-to-cascade ratios for the 1256.8- and 1420.5-keV levels shown in Table VI. (The Coulomb excitation data also suffers from this problem, which explains the apparent disagreement of their crossover-to-cascade ratio for the 1256.8-keV level with that of the present work.) Overall the agreement between the present results and the Coulomb excitation and neutron-scattering results is very good; the disagreements between our work and the neutron work for the 1536.4- and 2059.9-keV levels are due to unresolved transitions in the neutron work, in the first case to a second nearby level at 1537.6 keV (which is not populated in the radioactive decay) and in the second case to a crossover transition from a level at 1894 keV that cannot be resolved from the cascade transition from the 2059.9-keV level.

It is clear that for some states (1219.0, 1420.5, 1578.2, 1683.1 keV) the crossover transition dominates in intensity by an order of magnitude or more, suggesting that the $g_{7/2}$ state has a prominent role in those configurations. For other states (1381.4, 1476.5, 1761.2, 1856.6, and 1962.8 keV) the cascade transition dominates by an order of magnitude or more, and one concludes that the $d_{5/2}$ state may dominate those configurations. For the remaining states the ratio is of order unity, perhaps suggesting mixed configurations. More detailed theoretical calculations of the branching ratios may render these qualitative conclusions more quantitative.

## ACKNOWLEDGMENTS

The support of the staff and facilities of the Oregon State University Radiation Center in carrying out these experiments is acknowledged with gratitude. We are grateful to Professor E. B. Norman for the loan of a $^{56}$Co calibration source.

[1] F. Voss, K. Wisshak, K. Guber, F. Käppeler, and G. Reffo, Phys. Rev. C **50**, 2582 (1994).
[2] M. K. Murphy, R. K. Piper, L. R. Greenwood, M. G. Mitch, P. J. Lamperti, S. M. Seltzer, M. J. Bales, and M. H. Phillips, Med. Phys. **31**, 1529 (2004).
[3] P. Eberhardt, J. Geiss, and H. Graf, Earth Planet. Sci. Lett. **12**, 260 (1971).
[4] W. A. Kaiser and B. L. Berman, Earth Planet. Sci. Lett. **15**, 320 (1972).
[5] S. F. Mughabghab, *Atlas of Neutron Resonances: Resonance Parameters and Thermal Cross Sections Z = 1–100* (Elsevier, Amsterdam, 2006).
[6] EXFOR/CSISRS Experimental Nuclear Reaction Data, National Nuclear Data Center, Brookhaven National Laboratory [http://www.nndc.bnl.gov/exfor/exfor00.htm].
[7] See [http://radiationcenter.oregonstate.edu/].
[8] ORTEC, Inc. [http://www.ortec-online.com/pdf/a65.pdf].
[9] M. Berglund and M. E. Wieser, Pure Appl. Chem. **83**, 397 (2011).
[10] Evaluated Nuclear Structure Data File, National Nuclear Data Center, Brookhaven National Laboratory [http://www.nndc.bnl.gov/ensdf/].
[11] C. H. Wescott, W. H. Walker, and T. K. Alexander, *Proceedings of the Second United Nations International Conference on the Peaceful Uses of Atomic Energy, United Nations, Geneva*, 1958, Vol. 16, p. 70.
[12] P. A. Aarnio, J. T. Routti, and J. V. Sandberg, J. Radioanal. Nucl. Chem. **124**, 457 (1988).
[13] R. G. Helmer and C. van der Leun, Nucl. Instrum. Methods Phys. Res., Sect. A **450**, 35 (2000).
[14] K. Debertin and R. G. Helmer, *Gamma- and X-ray Spectrometry with Semiconductor Detectors* (North-Holland, Amsterdam, 1988), p. 224.
[15] P. Bode, J. J. Ammerlaan, and M. Koese, Appl. Radiat. Isot. **42**, 692 (1991).
[16] D. J. Horen, W. H. Kelly, and L. Yaffe, Phys. Rev. **129**, 1712 (1963).
[17] R. G. Wille and R. W. Fink, Phys. Rev. **118**, 242 (1960).
[18] R. J. Gehrke, Appl. Radiat. Isot. **31**, 37 (1980).
[19] R. S. Tilbury and H. H. Kramer, Nucl. Sci. Eng. **31**, 545 (1968).
[20] R. E. Heft, in *Conference on Computers in Activation Analysis*, edited by R. Farmakes (American Nuclear Society, La Grange Park, IL, 1968).
[21] W. S. Lyon, Nucl. Sci. Eng. **8**, 378 (1960).
[22] E. Steinnes, J. Inorg. Nucl. Chem. **34**, 2699 (1972).
[23] R. Van der Linden, F. De Corte, and J. Hoste, J. Radioanal. Chem. **20**, 695 (1974).
[24] J. St-Pierre and G. Kennedy, Nucl. Instrum. Methods Phys. Res., Sect. A **564**, 669 (2006).
[25] Yu. P. Gangrsky, P. Zuzaan, N. N. Kolesnikov, V. G. Lukashik, and A. P. Tonchev, Bull. Russ. Acad. Sci. Physics **65**, 121 (2001).
[26] H. S. Hans, M. L. Sehgal, and P. S. Gill, Nucl. Phys. **20**, 183 (1960).
[27] S. K. Mangal and P. S. Gill, Nucl. Phys. **41**, 372 (1963).
[28] S. Katcoff, Phys. Rev. **72**, 1160 (1947).
[29] S. M. Masyanov and V. A. Anufriev, At. Energ. **69**, 195 (1990).
[30] H. H. Kramer and W. H. Wahl, Nucl. Sci. Eng. **22**, 373 (1965).
[31] A. Foglio Para and M. Mandelli Bettoni, Energ. Nuclaire **14**, 228 (1967).
[32] S. E. Agbemava, R. B. M. Sogbadji, B. J. B. Nyarko, and R. Della, Ann. Nucl. Energy **38**, 379 (2011).
[33] M. D. Ricabarra, R. Turjanski, G. H. Ricabarra, and C. B. Bigham, Can. J. Phys. **46**, 2473 (1968).
[34] T. W. Burrows, Nucl. Data Sheets **92**, 623 (2001).
[35] J. C. Hill and M. L. Wiedenbeck, Nucl. Phys. A **119**, 53 (1968).
[36] G. Berzins, M. E. Bunker, and J. W. Starner, Nucl. Phys. A **128**, 294 (1969).
[37] R. E. Laird, Phys. Rev. C **17**, 1498 (1978).
[38] C. B. Zamboni, J. A. G. Medeiros, A. L. Lapolli, F. A. Genezini, S. P. Camargo, M. T. F. da Cruz, and J. Y. Zevallos-Chávez, Appl. Radiat. Isot. **55**, 477 (2001).
[39] R. A. Meyer, Fizika **22**, 153 (1990).
[40] D. E. Alburger and C. Wesselborg, Nucl. Instrum. Methods Phys. Res., Sect. A **423**, 49 (1999).
[41] V. A. Bondarenko *et al.*, Nucl. Phys. A **551**, 54 (1993).
[42] R. B. Firestone, S. F. Mughabghab, and G. L. Molnár, *Database of Prompt Gamma Rays from Slow Neutron Capture for Elemental Analysis* (International Atomic Energy Agency, Vienna, 2007), Chap. 5.
[43] M. Waroquier and K. Heyde, Nucl. Phys. A **144**, 481 (1970); K. Heyde and M. Waroquier, *ibid.* **167**, 545 (1971).
[44] J. Suhonen, J. Toivanen, A. Holt, T. Engeland, E. Osnes, and M. Hjorth-Jensen, Nucl. Phys. A **628**, 41 (1998).
[45] N. Yoshinaga, Y. D. Devi, and A. Arima, Phys. Rev. C **62**, 024309 (2000).
[46] R. G. Kulkarni and K. Andhradev, Can. J. Phys. **57**, 1940 (1979).
[47] M. R. Ahmed, S. Al-Najjar, M. A. Al-Amili, N. Al-Assafi, N. Rammo, A. M. Demidov, L. I. Govor, and Yu. K. Cherepantsev, *Atlas of Gamma-Ray Spectra from the Inelastic Scattering of Reactor Fast Neutrons* (Atomizdat, Moscow, 1978).
[48] J. M. Daniels and J. Felsteiner, Can. J. Phys. **46**, 1849 (1968).